Off-equatorial chorus occurrence and wave amplitude distributions as observed by the Polar Plasma Wave Instrument

N. L. Bunch,[1] M. Spasojevic,[1] and Y. Y. Shprits[2,3]

Received 4 October 2011; revised 8 February 2012; accepted 13 February 2012; published 6 April 2012.

[1] Determining the global distribution of chorus wave power in the off-equatorial region (i.e., magnetic latitude $\lambda > 15°$) is a crucial component of understanding the contribution of chorus to radiation belt acceleration and loss. In this paper we use a database of chorus power spectral density observations from the Plasma Wave Instrument (PWI) Sweep Frequency Receiver (SFR) on the Polar spacecraft to generate separate distributions of wave occurrence rate and magnetic field amplitude as a function of space and geomagnetic activity. Previous studies focused on a band-integrated and time-averaged data product to characterize the global distribution of wave power. Using a slightly different technique, we first estimate the wave amplitude from the peak wave power spectral density for times when chorus is observed. The mean wave amplitude at a given location is then multiplied by the wave occurrence rate to yield the time-averaged amplitude. We present the spatial distributions of wave occurrence rate, mean amplitude, and time-averaged amplitude in the region of maximum statistics, $\lambda > 15°$ and $R = 4-8\ R_E$. We find that waves of significant amplitude (>10 pT) can be observed in all local time sectors, but significant wave occurrence (>20%) is confined to the dawn and noon local time sectors. Wave mean and time-averaged amplitudes are also highest in the dawn and noon sectors. The spatial extent of regions with high time-averaged amplitude is primarily defined by regions of high occurrence rate. Time-averaged amplitudes exceeding ~6 pT are observed up to a magnetic latitude of 40° at dawn and 50° at noon, while at midnight and dusk the time-averaged amplitude tends to be below that value. We also examine the geomagnetic and solar wind dependence of the spatial distribution of wave occurrence, mean amplitude, and time-averaged amplitude. In the off-equatorial region ($\lambda > 15°$), wave amplitude and occurrence on the nightside increase dramatically during disturbed geomagnetic and solar wind conditions. In contrast, waves on the dayside occur over a wider range of activity, and even during quiet conditions, mean and time-averaged amplitudes at noon significantly exceed amplitudes at midnight for disturbed times. In the dusk sector, observation of waves is mostly limited to quiet conditions, and during those times, mean amplitudes at dusk exceed those at midnight and approach amplitudes observed in the dawn sector. Parallel investigation of the independent variability of occurrence and amplitude provides a more complete picture of the chorus wave environment, particularly for application to modeling radiation belt dynamics on both short and long time scales.

Citation: Bunch, N. L., M. Spasojevic, and Y. Y. Shprits (2012), Off-equatorial chorus occurrence and wave amplitude distributions as observed by the Polar Plasma Wave Instrument, *J. Geophys. Res.*, *117*, A04205, doi:10.1029/2011JA017228.

1. Introduction

[2] The distribution of relativistic electrons that form the Earth's outer radiation belt is extremely variable with the trapped flux varying by orders of magnitude on time scales of hours to days [e.g., *Li et al.*, 2001; *Friedel et al.*, 2002; *Reeves et al.*, 2003]. The dynamic evolution of electron fluxes is controlled by competition among a host of acceleration and loss processes [*Shprits et al.*, 2008a, 2008b], and the relative contribution of individual processes is not fully understood. The role of wave-particle interactions involving whistler mode chorus waves is particularly confounding

[1]Space, Telecommunications, and Radioscience Laboratory, Stanford University, Stanford, California, USA.
[2]Institute of Geophysics and Planetary Physics, University of California, Los Angeles, California, USA.
[3]Department of Atmospheric Sciences, University of California, Los Angeles, California, USA.

0148-0227/12/2011JA017228

since these waves can contribute to both electron acceleration and loss [*Bortnik and Thorne*, 2007, and references therein]. Pitch angle scattering by chorus can result in the loss of electrons over a wide range of energy, ranging from hundreds of eV to >1MeV [*Ni et al.*, 2008; *Thorne et al.*, 2005]. Chorus waves are also a driver of energy diffusion, which can result in the acceleration of seed electrons with energies of tens to hundreds of keV to energies of 1 MeV or greater [*Horne et al.*, 2003b; *Albert et al.*, 2009; *Shprits et al.*, 2008b]. In fact, there is growing scientific consensus that stochastic electron acceleration by chorus may be the dominant mechanism acting during relativistic electron enhancements in the outer radiation belt [*Thorne*, 2010].

[3] Diffusion theory is one of the primary methods used in studies of the global evolution of radiation belt electron distributions [*Schulz and Lanzerotti*, 1974, and references therein]. Numerical simulations of this kind treat wave-particle interactions as a quasi-linear (QL) diffusive process that can transport electrons in both energy and pitch angle [e.g., *Albert et al.*, 2009; *Subbotin et al.*, 2010]. Techniques are available for computing the required diffusion coefficients [e.g., *Summers*, 2005; *Shprits et al.*, 2006], but the fundamental unknown quantity in the determination of resonant energies and rates of diffusion is the global distribution of wave power as a function of radial distance, magnetic latitude, local time, spectral extent, wave normal angle, and solar wind and magnetospheric driving conditions.

[4] First definitively measured in situ by *Burtis and Helliwell* [1969], the spectral extent and upper band of banded chorus was first discussed by *Tsurutani and Smith* [1974], who noted that the spectrum of equatorial chorus often exhibited an apparent null near 0.5 times the local gyrofrequency. *Burtis and Helliwell* [1976] then reported a similar result by statistically showing that the center frequency of chorus has a bimodal distribution, which they termed as upper or lower band for that lying above or below 0.5 times the equatorial gyrofrequency.

[5] Further investigation by *Tsurutani and Smith* [1977] also found chorus in the outer magnetosphere to reside primarily in the lower band. However, in the outer dayside region, where the solar wind ram pressure causes the magnetic minima to shift away from the equator, observations revealed a double peaked distribution within the lower band. Because of the correspondence of the frequency of this additional lower band peak with the minimum gyrofrequency of the field line, rather than the local or equatorial gyrofrequency, they suggested that this was evidence of chorus being generated in "minimum B pocket" regions in the outer dayside. Statistics provided by modern equatorial satellite missions have helped to confirm and extend the results of *Burtis and Helliwell* [1976] and *Tsurutani and Smith* [1977] by coarsely determining the relative prevalence of upper and lower band chorus in this region [e.g., *Meredith et al.*, 2001, 2003a; *Santolík et al.*, 2005a]. Further, when combined with recent theoretical work, multicomponent measurements have found banded structure of chorus to follow the gyrofrequency in the generation region [*Trakhtengerts et al.*, 2007; *Santolík et al.*, 2008].

[6] Along with spectral extent, wave normal angle directly impacts the electron energies and pitch angles with which chorus interacts, and recent statistical studies have contributed to separately characterizing the global distribution of upper and lower band chorus wave normals in the equatorial region [*Li et al.*, 2011a, 2011b] and as a function of geomagnetic latitude [*Haque et al.*, 2010].

[7] Since the most recent interest in chorus emissions has shifted toward wave-particle interactions, the nature of studies defining the global distribution of chorus activity has shifted from limited probability and intensity statistics [e.g., *Tsurutani and Smith*, 1974, 1977] to time-averaging integrated chorus wave power [e.g., *Meredith et al.*, 2001, 2003c], which is used as the key chorus wave parameter entered in modern diffusion codes. This approach involves integrating chorus wave power across a frequency band defined, assuming field aligned propagation, as typically 0.1 to ~0.5 times the equatorial gyrofrequency (Ω_{ce-eq}), and averaging this number in time. Time averaged wave power can also be thought of as the product of typical wave intensity and its occurrence rate, so as to encompass both wave amplitude and probability in a single data product. As increasing evidence has mounted that enhancements in outer radiation belt fluxes are driven by processes internal to the magnetosphere [*Li et al.*, 1997], inclusion of time-averaged wave amplitudes for various types of magnetospheric waves has led us to begin to understand the relative contribution of different wave-particle interactions, such as with chorus, hiss, and electromagnetic ion cyclotron (EMIC) waves, to radiation belt acceleration and loss [*Shprits et al.*, 2008b]. In practice, chorus is modeled in radiation belt codes by using parameterizations of band-integrated wave amplitudes (B_w) [*Meredith et al.*, 2001, 2003c; *Shprits et al.*, 2007], where wave power is assumed distributed across a Gaussian power spectrum bounded by the chorus frequency band (e.g., ~0.1–0.5Ω_{ce-eq} for lower band chorus) [e.g., *Tsurutani and Smith*, 1974; *Burtis and Helliwell*, 1976], and is a function of geomagnetic conditions and magnetospheric location.

[8] Because of the prevalence of wave observations from equatorially orbiting satellites, and their proximity to the assumed generation region, there has been a focus on generating spatial distribution maps of chorus activity, now covering much of the equatorial magnetosphere, ranging from ~2–10 R_E [*Koons and Roeder*, 1990; *Meredith et al.*, 2001; *Li et al.*, 2009]. Although studies using equatorially orbiting satellites have produced some observations ranging as high as ~30° magnetic latitude (λ), statistics at $\lambda > 15°$ are comparatively sparse, and until recently early statistics presented by *Tsurutani and Smith* [1977] represented the most comprehensive characterization of off-equatorial chorus to date. Recent radiation belt model results have shown that chorus extending significantly away from the equator (>30°) can dramatically increase diffusion rates, particularly for pitch angles <40°, and that better statistical characterization of chorus in the off-equatorial region is needed [*Shprits et al.*, 2006; *Orlova and Shprits*, 2010]. For example, *Shprits et al.* [2006] showed that energy and pitch angle diffusion coefficients for pitch angles of 20°–40° for 1 MeV electrons at $L = 3.5$ can shift from being negligible when considering only equatorially confined waves ($\lambda < 15°$), to ~10^{-5} s^{-1} (similar to that for pitch angles >40°) by extending waves to just 25° latitude. Studies by *Sigsbee et al.* [2010] and *Bunch et al.* [2011] have begun to address this need and have shown significant chorus occurrence rates and intensities, respectively, in the off-equatorial region by employing observations from the Plasma Wave

Instrument (PWI) onboard the Polar spacecraft, the polar orbit of which (~18 h, ~2 × 9 R_E, ~90° inclination, North Pole apogee) has allowed for extension of the known distribution of chorus activity to much higher latitudes.

[9] The study by *Bunch et al.* [2011] used the Polar PWI database to define the latitudinal extent of chorus, and found that waves with significant spectral density are routinely observed ranging to $\lambda = 55°$ around noon, 40° at dawn, and 25° at midnight, and vary significantly in intensity as a function of magnetic local time (MLT), L^*, λ and geomagnetic conditions. *Bunch et al.* [2011] also showed that the highest-latitude chorus observation for each half orbit also followed the local time trend of increasing from midnight to noon, suggesting that when intense chorus is generated, it is often observed as if it were filling a volume in space, a feature that has not been quantified but is often notable in spectrograms for Polar perigee passes where chorus is observed. They go on to show that within the orbital constraints of the study, resonant energies in a realistic magnetosphere suggest that wave-particle interactions near this high-latitude region are favorable for interaction with MeV electrons from 04:00 to 10:00 MLT, and $L^* < 7$. This region is consistent with the region of most observed MeV microburst precipitation [*O'Brien et al.*, 2004].

[10] Despite a history of investigation of the interaction between particles and single wave packets or chorus elements and structures [e.g., *Inan et al.*, 1978; *Albert*, 1993; *Albert et al.*, 2009; *Lakhina et al.*, 2010], global radiation belt codes typically consider all wave-particle interactions to be a quasi-linear diffusive process because of the difficulty of modeling this microphysics on a global scale. *Tsurutani et al.* [2011] recently showed that chorus at off-equatorial latitudes can have varying levels of coherence when observed significantly away from the source region, such that the elemental structure may erode because of dispersion as it propagates and also mix with counterpropagating waves once reflected. This type of propagation and subsequent mixing and erosion of chorus structures is also thought to be the mechanism responsible for producing hiss in the plasmasphere [e.g., *Bortnik et al.*, 2008]. Despite the fact that structured chorus propagates to, and is frequently observed at ground level [e.g., *Sazhin and Hayakawa*, 1992; *Golkowski and Inan*, 2008; *Golden et al.*, 2010, 2011], *Tsurutani et al.* [2011] argue that the lower coherence of chorus at off-equatorial latitudes lacks the fine temporal (~0.5 s) structure to explain MeV microburst precipitation with durations of <1 s. *Tsurutani et al.* [2009] and *Lakhina et al.* [2010] showed that coherent chorus elements near the equator could cause pitch angle transport and thus microburst precipitation of 10–100 keV electrons; however, rapid scattering of higher energies is not well understood. If MeV microburst is a result of fast scattering of electrons with chorus near the equator, one would expect microbursts to be more prominent on the nightside since in that local time sector high-intensity waves (>300 pT) occur most frequently [*Li et al.*, 2009, 2011a, 2011b]. Despite these apparent inclinations toward nighttimes, the L and MLT distribution of MeV microburst precipitation is most consistent with regions favorable for chorus wave-particle interactions on the dayside at off-equatorial latitudes [*Lorentzen et al.*, 2001; *O'Brien et al.*, 2003; *Thorne et al.*, 2005; *Bunch et al.*, 2011]. This all points to the ultimate need of better characterization of wave properties, as well as improved wave-particle interaction modeling in the off-equatorial region.

[11] In this paper we expand upon the work of *Bunch et al.* [2011] by statistically characterizing chorus in the off-equatorial region by generating spatially distributed maps of chorus occurrence probability and mean amplitude, and investigate how independent variations in their distributions contribute to those of time-averaged wave amplitude. This parallel investigation of the independent variability of occurrence and amplitude provide a more complete picture of the chorus wave environment as it pertains to modeling radiation belt dynamics on short and long time scales. Distributions are then each examined over a range of geomagnetic conditions to better elicit the drivers or predictors of chorus activity in different magnetospheric regions. These results provide the best estimates to date of off-equatorial chorus characteristics for direct inclusion in radiation belt diffusion models.

[12] Section 2 outlines the methods used for chorus event selection and amplitude estimation. Section 3 presents statistical and observational results derived from the chorus database, while section 3.1 discusses statistical distributions of chorus power spectral density, amplitude, and spectral extent; section 3.2 discusses the spatial distribution of chorus occurrence, sections 3.3 and 3.4 discuss the spatial distribution of mean and time-averaged chorus amplitude, respectively, and section 3.5 considers the variation of these parameters with respect to geomagnetic conditions. Section 4 places these results in the context of previous and future work. Section 5 summarizes our primary results and conclusions.

2. Method

[13] The Polar PWI included a Sweep Frequency Receiver (SFR) that provides continuous (~32 s resolution), single-component electric (E) and magnetic (B) field measurements in a log-spaced frequency mode (26 Hz to 810 kHz). In the frequency range where chorus is typically observed (200 Hz to 12.5 kHz), the SFR-obtained field measurements in two bands (200–1600 Hz and 1.6–12.5 kHz) each with 32 log spaced frequencies sampled at a cadence of 16.5 and 8.2 s per sweep, respectively [*Gurnett et al.*, 1995]. Chorus can be observed in SFR data during ascending and descending segments of the orbit and appears as a banded emission approximately following below 0.5 of the estimated equatorial gyrofrequency. Only chorus exclusively outside of the plasmasphere has been included in this study. The location of the plasmapause was inferred from the upper hybrid resonance [*Mosier et al.*, 1973; *Sigsbee et al.*, 2008, 2010], as well as observation of plasmaspheric hiss [*Dunckel and Helliwell*, 1969; *Russell et al.*, 1969; *Thorne et al.*, 1973]. Many examples of discrete or chorus-like waves inside the plasmasphere are observed, but analysis of such emissions is beyond the scope of this study. The spacecraft typically traverses the magnetic equator inside the plasmapause, and thus observations are most abundant in the northern hemisphere for $\lambda > 15°$ at radial distances of 4 to 8 R_E. In addition, intervals of cross talk, interference, and high noise levels, such as those caused by eclipse or interference from

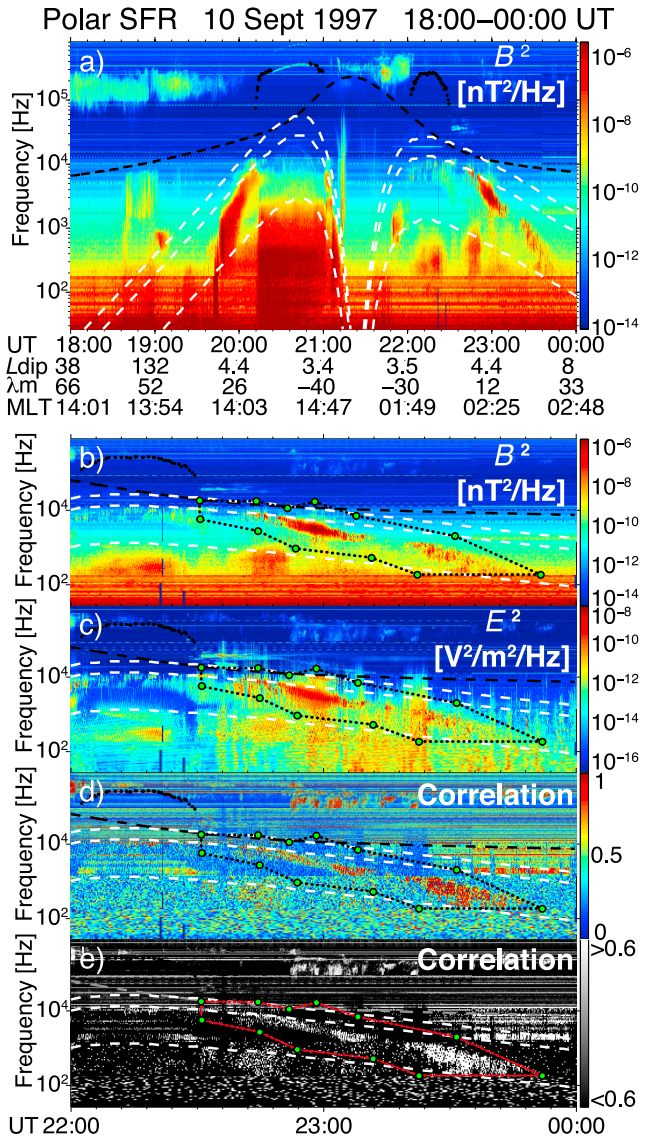

Figure 1. (a) Polar Sweep Frequency Receiver (SFR) spectrogram for a perigee pass in the ~14:00/02:00 MLT plane on 10 September 1997. The dashed black line is the locally measured f_{ce}, and dashed white traces are 1, 0.5, and 0.05 times the dipole equatorial f_{ce}. Black dots are the upper hybrid frequency, inferred from wave data in high-density regions. Chorus emissions are the banded electromagnetic waves between the top and bottom dashed white lines at 19:35–20:10, 21:50–22:00, and 22:30–00:00 UT. (b–e) For 22:00–00:00 UT, frequency-time plots of magnetic and electric power spectral density and associated correlation values in color scale and black and white across a value of 0.6. The data selection region is bounded by green circles and black dotted lines.

the Electric Field Instrument, are excluded from the database.

[14] Chorus intervals were selected by visual inspection of full resolution SFR spectrograms of E and B power spectral density. We found this approach most appropriate for the data set in part because chorus lies outside its expected bounds because of distortion of the outer magnetosphere where Polar often samples, as well as the ability to distinguish chorus from other waves that inhabit the chorus band, such as hiss as well as electrostatic and magnetosonic waves. An example chorus event selection is shown in Figure 1. As seen in Figure 1a, approaching perigee the spacecraft is inside the plasmasphere from about 20:15 to 21:05 UT and again after perigee from 22:00 to 22:30 UT. Figures 1b and 1c show B and E power spectral densities observed during an ascending orbit interval in the postmidnight sector. An interval of chorus is identified and bounded by green circles and black dotted lines. In order to ensure that the selected emissions are electromagnetic in nature, the data are filtered by the output of the SFR onboard correlator [cf. *Mellott et al.*, 1986; *Gurnett et al.*, 1995]. An example output from the SFR correlator is shown in Figure 1d. Correlation between the E and B channels is given on a scale between 0 and 1, where the correlation between a waveform and itself equals 1. A threshold correlation value of 0.6 was selected for this study (a natural break at high correlation). Thus, time periods where exclusively electric or magnetic field data were measured are excluded. Figure 1e shows a filtered version of Figure 1d, such that f-t elements with correlation greater than 0.6 are colored white, and those within the manually selected frequency-time region are selected for the database.

[15] Figure 2a shows the nominal frequency range of chorus observable by Polar as a function of the radial distance to the equatorial field crossing, R_0, and MLT, using the *Tsyganenko and Sitnov* [2005] (hereafter TS05) magnetic field model with moderate solar wind dynamic pressure, P, of 3 nPa. Following *Burtis and Helliwell* [1976], the upper and lower frequency bounds correspond to 0.95 and 0.05 times the minimum gyrofrequency of the field line. We use the simplifying assumption of propagation parallel to the field line, though cross field propagation, particularly at higher latitudes, may impact the effective bandwidth. Because of the high noise floor of the SFR B field measurement at frequencies below 200 Hz (see Figures 1a and 1b), indicated by the black dashed line in Figure 2a, only chorus above 200Hz is included (also employed by *Sigsbee et al.* [2008]). Although the very lowest expected frequency components of chorus are undetectable by the Polar PWI for $R_0 > 6$, even at the largest values of R_0 more than 60% of the chorus frequency band is detectable at all MLT.

[16] This approach allows for separation of chorus intervals from nonchorus intervals and the investigation of typical wave intensity, frequency extent, and occurrence patterns. Moreover, the combination of such parameters will prove useful in future development of radiation belt codes which include advection, as well as nonlinear terms and pitch angle transport, which rely on not just average amplitudes but probability of encountering waves with various characteristics [e.g., *Albert and Bortnik*, 2009; *Lakhina et al.*, 2010]. In fact, recent studies indicate that the relative coherence of waves may not only play an important role in modeling the QL diffusion process but may also lead to additional pitch angle transport because of discrete interactions with coherent or semicoherent waves [*Lakhina et al.*, 2010; *Tsurutani et al.*, 2011].

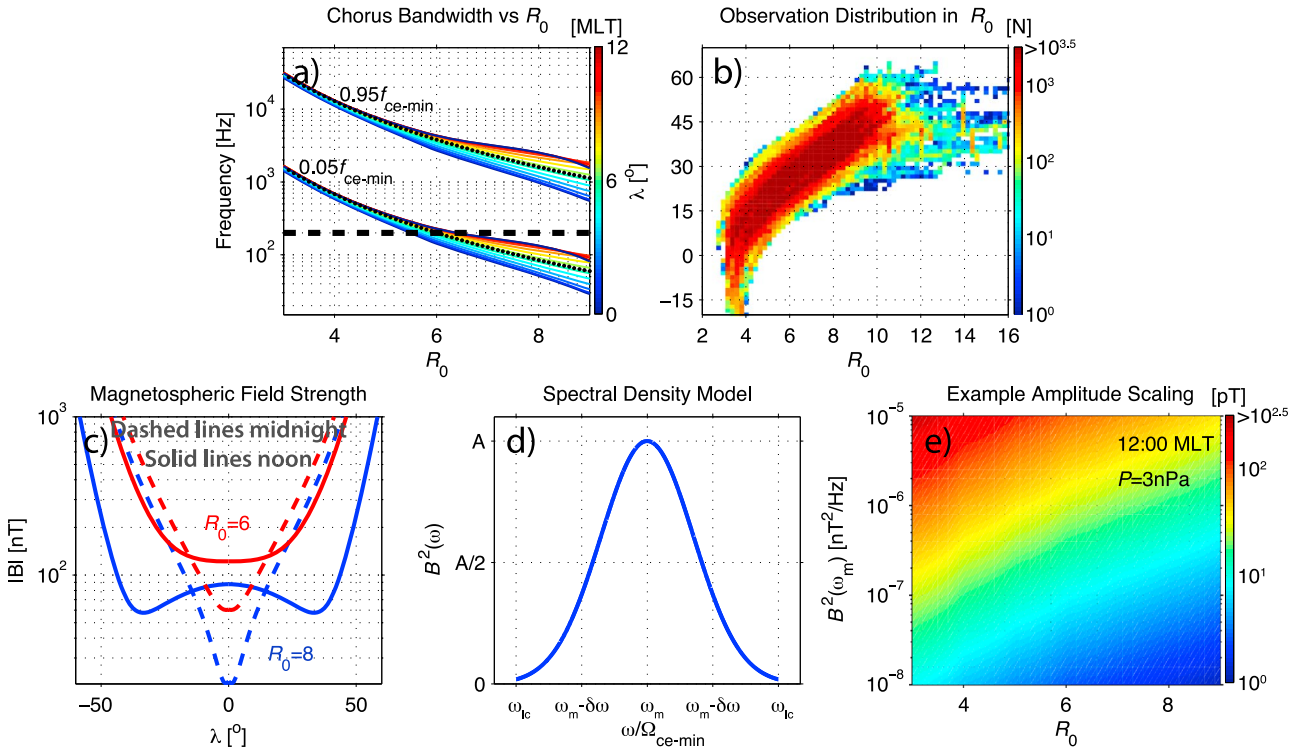

Figure 2. (a) Typical frequency bounds for chorus as a function of R_0. The upper frequency limit corresponds to $0.95f_{ce}$ of the magnetic field line minima, while the lower limit is represented by $0.05f_{ce}$. The black dotted line represents the calculation using a dipole field model. The dashed black line indicates low-frequency cutoff due to noise considerations. (b) Distribution of chorus observations by Polar in magnetic latitude and R_0. (c) Magnetic field line strength as a function of magnetic latitude for R_0 = 6, 8. Solid lines are for noon, and dashed lines are for midnight. (d) Assumed power spectral density as a function of normalized frequency used in wave amplitude estimates. (e) Example conversion matrix from power spectral density to wave amplitude for a range of R_0 at 1200 MLT and P = 3 nPa.

[17] Chorus was resolved by the SFR on 459 out of 1388 half orbits between 25 Mar 1996 and 16 September 1997 for a total of 584,811 frequency-time (*f-t*) spectral density elements for use in statistical analysis. For each *f-t* element, the R_0 value and minimum gyrofrequency along the field line were calculated using the ONERA-DESP library and the TS05 magnetic field model and the concomitant solar wind parameters [*Qin et al.*, 2007]. Figure 2b shows the region of space, in R_0 and magnetic latitude, λ, where Polar observed chorus. Polar observed chorus from $|\lambda|$ = 0 to 63°, and from R_0~3 to as high as ~16. A major reason for using Polar for this study is to survey underinvestigated regions of space, particularly magnetic latitudes >30°. However, the polar orbit of the spacecraft does pose significant challenges in characterizing the distribution of observed waves since latitude and R_0 are constrained together as shown in Figure 2b. For example, Polar best samples R_0 from 3–5 at latitudes below 15°. Observations at latitudes of 15°–30° best correspond to R_0 of 3–8, 30°–45° best corresponds to R_0 of 4–9, and 45°–60° best covers R_0 of 7–9. Results presented here will mainly focus on observations at latitudes >15°.

[18] We note that the choice of field line or drift shell mapping in the off-equatorial region, particularly in the outer dayside, can be difficult and often unreliable. Various parameters are often used to order data, such as dipole L, L_m [*McIlwain*, 1966], L^* [*Roederer*, 1970], and R_0. We find that R_0, representing the radial distance to the equatorial field line crossing found here using the TS05 field model, provides a physically intuitive framework from which to describe the observed wave distributions, and is used throughout this paper.

[19] Using the database of chorus spectral densities, we derive distributions of chorus occurrence rate by dividing the total time duration of chorus observed in a given spatial bin by the total orbital dwell time of the spacecraft in that bin. This has been done at the time resolution of the SFR (~32 s) using a bin size of R = 0.25 R_E, and λ = 5°.

[20] Next, we use the database of spectral densities to approximate the integrated chorus wave amplitude. This is done at the time resolution of the SFR using measured spectral densities along with an assumption of spectral distribution. Current convention for modeling the chorus spectrum involves an assumption that the frequency distribution of chorus wave power is approximately Gaussian [e.g., *Burtis and Helliwell*, 1976; *Horne et al.*, 2003, 2005; *Summers*, 2005; *Shprits et al.*, 2006] given by

$$B^2(\omega) = A^2 \exp\left[-\left(\frac{\omega-\omega_m}{\delta\omega}\right)^2\right], \quad (1)$$

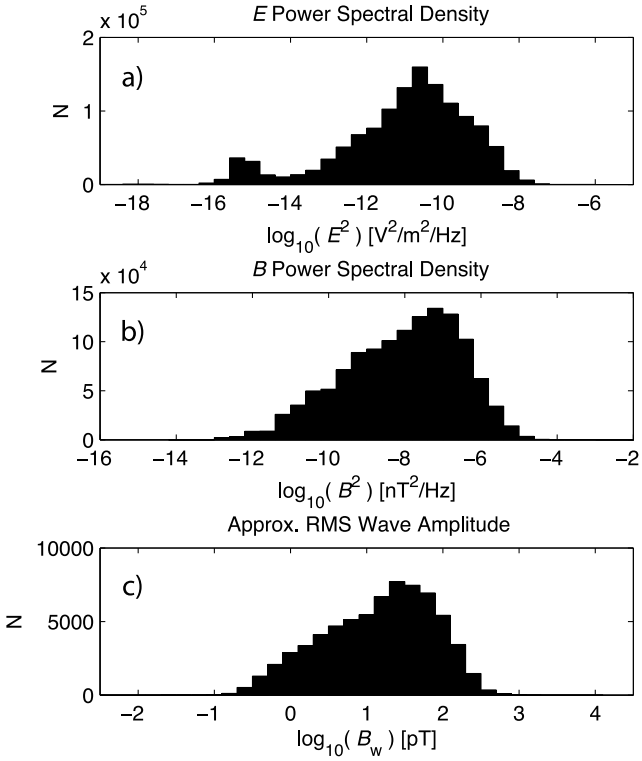

Figure 3. Histograms of chorus (a) electric and (b) magnetic field power spectral densities observed by Polar SFR for $\lambda > 15°$. (c) Histogram of chorus approximate RMS magnetic wave amplitude for $\lambda > 15°$.

where $B^2(\omega)$ is the power spectral density of the chorus magnetic field (in nT^2/Hz) as a function of wave frequency, ω_m is the frequency of maximum wave power, and $\delta\omega$ is the bandwidth. The normalization constant, A, is given by

$$A^2 = \frac{|B_w|^2}{\delta\omega}\frac{2}{\sqrt{\pi}}\left(\mathrm{erf}\left(\frac{\omega_m-\omega_{lc}}{\delta\omega}\right)+\mathrm{erf}\left(\frac{\omega_{uc}-\omega_m}{\delta\omega}\right)\right)^{-1}, \quad (2)$$

where B_w is the RMS wave amplitude input (in nT), ω_{uc} and ω_{lc} are the upper and lower frequency cutoffs, and the wave spectrum is zero outside of $\omega_{uc} < \omega < \omega_{lc}$. The frequency range is typically scaled as a function of the equatorial gyrofrequency, and the model can be adapted to correspond to the frequency range of upper band chorus ($\omega_m > 0.5\Omega_{ce-eq}$), lower band ($\omega_m < 0.5\Omega_{ce-eq}$), both upper and lower band, or chorus not exhibiting a null.

[21] We note here that, although for most parts of the magnetosphere they are equivalent, in this study we chose to use the minimum field line gyrofrequency, rather than the coordinate system defined equatorial gyrofrequency, as our guide for chorus frequency. Figure 2c shows that on the dayside for moderate driving pressure (e.g., $P = 3$ nPa) for $R_0 > 6$ the field line minimum B begins to bifurcate toward locations above and below the equator. The choice of B_{min} is primarily driven by theoretical considerations since it is at this location that resonant energies are minimized and pitch angle anisotropies are maximized, both of which favor wave growth [*Kennel and Petschek*, 1966]. There is also some observational evidence supporting the idea of generation in the off-equatorial minimum-B region [*Tsurutani and Smith*, 1977; *Vaivads et al.*, 2007; *Menietti et al.*, 2009].

[22] Various parameterizations for the spectral extent of chorus, illustrated in Figure 2d, have been used in previous radiation belt models. Depending on spatial and geomagnetic considerations, frequency limits as broad as 0.05–$0.95\Omega_{ce}$ and as narrow as 0.1–$0.3\Omega_{ce}$ have been used with values of $\delta\omega$ ranging from 0.1 to $0.3\Omega_{ce}$ and ω_m from 0.2 to $0.6\Omega_{ce}$. In this study, we follow a spatially uniform model commonly used for describing lower band chorus [*Summers*, 2005; *Summers et al.*, 2007; *Shprits et al.*, 2006; *Horne and Thorne*, 2003; *Horne et al.*, 2005], where $\omega_m = 0.35\Omega_{ce-min}$, $\delta\omega = 0.15\Omega_{ce-min}$, $\omega_{lc} = 0.05\Omega_{ce-min}$, and $\omega_{uc} = 0.65\Omega_{ce-min}$ [e.g., *Burtis and Helliwell*, 1976; *Meredith et al.*, 2001]. These values are consistent with initial estimates of the chorus frequency distribution observed by Polar. A detailed analysis of the spectral distribution of Polar observations of chorus is the subject of a forthcoming manuscript.

[23] Therefore, to estimate the total wave magnetic field amplitude, we set the value of $B^2(\omega_m)$ to the measured spectral density (*f-t*) element with highest intensity for each interval. Using the selected values of ω_m, $\delta\omega$, ω_{lc}, and ω_{uc}, the expression for chorus magnetic wave amplitude B_w reduces to

$$B_w = \left[(0.15\Omega_{ce-min})\sqrt{\pi}\,\mathrm{erf}(2)B^2(\omega_m)\right]^{1/2}. \quad (3)$$

[24] Figure 2e shows an example of the scaling of magnetic power spectral density to magnetic wave amplitude for a range of R_0 and spectral density at 12:00 MLT for $P = 3$ nPa. This framework, when compared to extreme cases for the bandwidth ranging from $\delta\omega = 0.1\Omega_{ce-eq}$ to a constant spectral density across the band, we estimate the bound for potential systematic error in wave amplitude (power) estimation of this type to be ~40% (60%). We consider this acceptable for the purpose of this investigation since this is found to be smaller than the statistical uncertainty of the wave power and spectral density distributions (i.e., standard deviation or interquartile range), which are around an order of magnitude (see section 3.1).

[25] The final data product that is computed is the time-averaged wave power, which is the wave occurrence rate multiplied by the mean wave amplitude at each spatial location.

3. Data Presentation

3.1. Basic Statistics

[26] Figure 3 shows histograms of the measured electric (Figure 3a) and magnetic (Figure 3b) field power spectral densities of chorus for $\lambda > 15°$. One may note that the tail of observations at lower spectral densities falls off regularly for B^2, but E field spectral densities appear to pile up around 10^{-15} $V^2/m^2/Hz$. This appears to be due to selection of coherent emissions that are detectible in E but are barely above the typical noise level of the magnetic loop antenna (~10^{-13} nT^2/Hz). Also, the sharp drop-off of the histogram at high spectral densities may be an effect of the integration time of the SFR at each frequency. Although there are reports of chorus subpackets ranging to much higher amplitudes (>1 nT) [*Santolík et al.*, 2003; *Cattell et al.*, 2008; *Cully et al.*, 2008b; *Tsurutani et al.*, 2009], such peaks occur on time scales of ~100 ms and are unlikely to

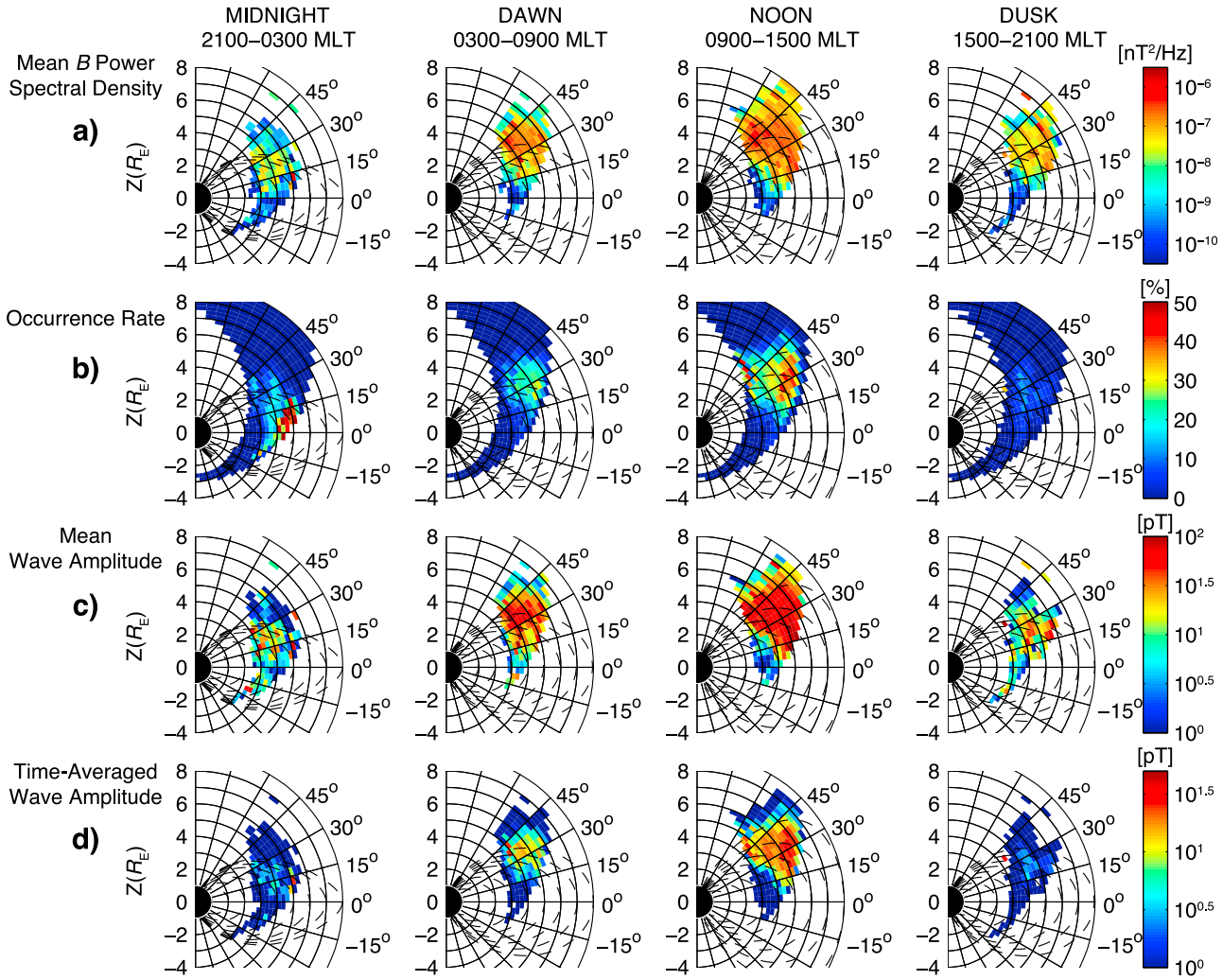

Figure 4. Spatial distributions of (a) mean magnetic spectral density, (b) observed occurrence rate, (c) mean wave amplitude, and (d) time-averaged wave amplitude, binned in R = 0.25 R_E and λ = 5°, for midnight (21:00–03:00 MLT), dawn (03:00–06:00 MLT), noon (09:00–15:00 MLT), and dusk (15:00–21:00 MLT) local time sectors. Field lines are for P = 3 nPa using TS05.

be observed at SFR integration times of ~260 ms to 1 s. Figure 3c shows a histogram of chorus wave amplitudes estimated from the power spectral densities, as described in section 2, for $\lambda > 15°$. The distribution peaks in the tens of pT and ranges into the hundreds of pT, which is consistent with observations made in the equatorial region by CRRES and THEMIS [e.g., *Meredith et al.*, 2001; *Li et al.*, 2007].

[27] Figure 4a shows the distribution of chorus mean B power spectral density binned as a function of R and λ. Although this study is primarily concerned with waves for $\lambda > 15°$, we present all available data, including those for $\lambda < 15°$. These distributions, described in detail by *Bunch et al.* [2011], show a dominance of wave power at dawn and noon, with the latitudinal extent of chorus increasing from midnight to noon.

3.2. Chorus Occurrence Rate

[28] Figure 4b shows the derived distribution of chorus occurrence in the same format as Figure 4a. In the midnight sector, occurrence rates of >40% are observed for $R_0 > 5$ and $\lambda < 15°$, consistent with previous reports [*Tsurutani and Smith*, 1977; *Meredith et al.*, 2001; *Li et al.*, 2009] while for $\lambda > 15°$ occurrence drops to below 20%. In the dawn sector for $\lambda > 15°$, occurrence rates are in the range of 15%–30%. The noon sector shows both the greatest rate of occurrence as well as the largest spatial region of occurrence within the orbital coverage of Polar with rates maximizing near 50% between 15° and 45°. The dusk sector shows the lowest occurrence rate, maximizing below 20%.

3.3. Mean Wave Amplitude

[29] Magnetic wave amplitude distributions shown in Figure 4c have a similar character to those of power spectral density (Figure 4a). The strongest waves appear in the noon and dawn sectors. Note here that because of the difference in chorus bandwidth from the inner to outer magnetosphere (Figure 2a), spectral densities at high R_0 correspond to lower wave amplitudes compared to similar spectral densities at lower R_0 values.

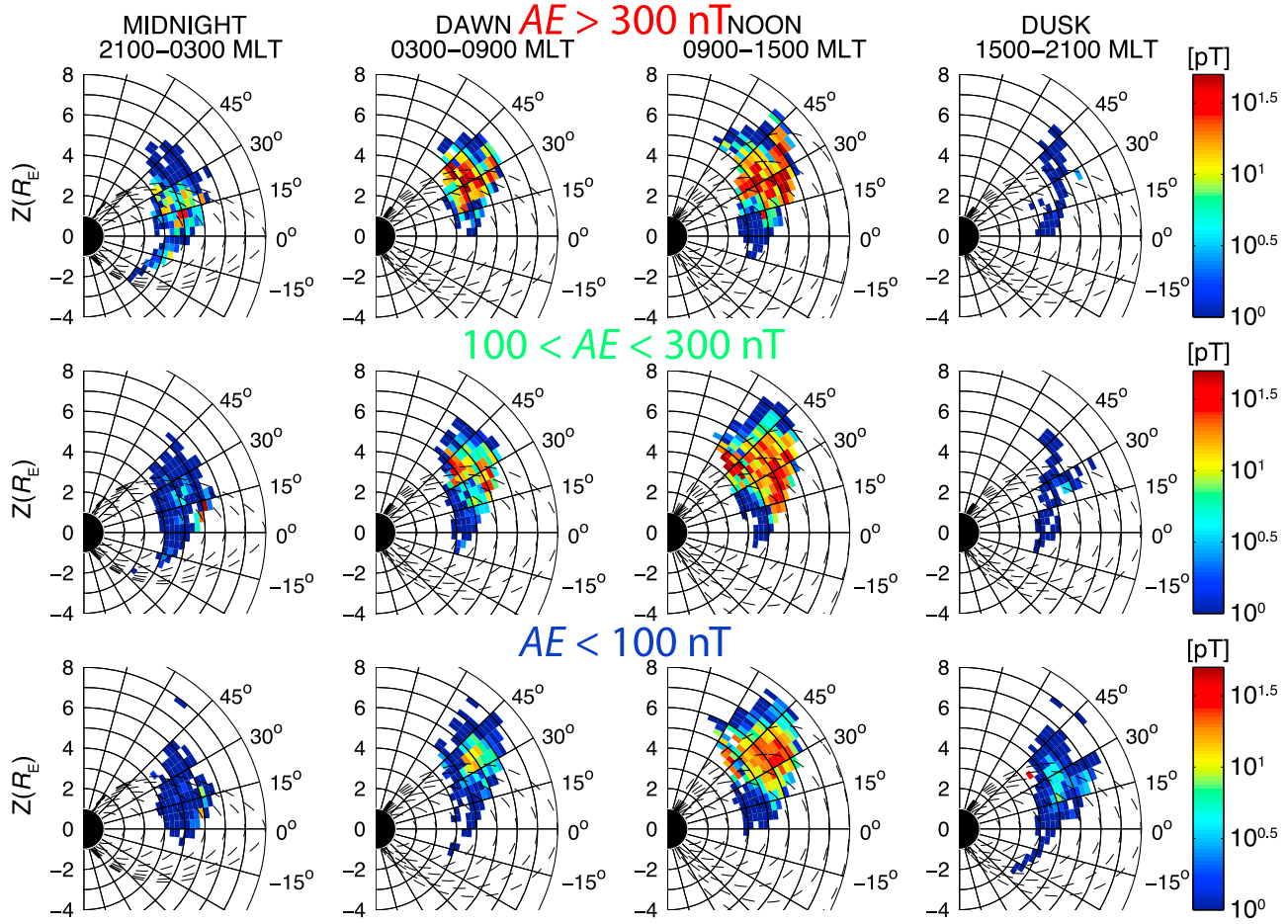

Figure 5. Substorm dependence of time-averaged chorus wave amplitude.

[30] The region in the dawn and noon sectors showing greatest mean amplitude (~100 pT) lies between ~15° and 45°, where Polar intersects field lines for $R_0 > 6$. Studies from both CRRES and THEMIS [e.g., *Meredith et al.*, 2003c; *Li et al.*, 2009] also found the most intense waves in this region up to the latitudinal limit of the orbital coverage (<30° and <25°, respectively). The region of greatest wave amplitude at midnight is confined below 30° latitude across the sampled R space. This is consistent with observations by THEMIS which also found strong confinement of waves at midnight to the equatorial region [*Li et al.*, 2009, 2011a]. THEMIS also found the most intense waves (>100 pT) in the equatorial region to reside in the midnight sector at ~6–8 R_E, and though they are outside of Polar's sampling near the equator (~3–5 R_E) waves amplitudes at midnight do appear to maximize near $R_0 \approx 7$. At dusk the highest amplitudes appear between 15° and 30° latitude outside of $R_0 \approx 6$.

3.4. Time-Averaged Wave Amplitude

[31] The time-averaged chorus amplitude is computed by multiplying the occurrence rate by the mean wave amplitude and the spatial distributions are shown in Figure 4d. In the midnight sector, despite moderate mean amplitudes up to $\lambda \approx 30°$, time-averaged amplitudes are low throughout because of the low rate of occurrence. Despite an increased occurrence rate at equatorial latitudes, time-averaged amplitudes are fairly low because of the low mean amplitudes. This appears consistent with observations by THEMIS at midnight which show waves to be primarily confined near the equator and between 6 and 8 R_E (outside of Polar's sampling of the equatorial region of ~3–5 R_E). Both occurrence and mean amplitude statistics at high latitude are highest in the dawn and noon time sectors resulting in the highest time-averaged wave amplitudes, also consistent with previous results [*Meredith et al.*, 2001, 2003c; *Li et al.*, 2009]. At dawn moderate time-averaged amplitudes are observed as high as $\lambda = 50°$, though this latitude is lower than the edge of the mean amplitude distribution because of the lower occurrence rate at $\lambda > 40°$. In the noon sector the region of significant time-averaged amplitude is also "trimmed" in size compared to the distribution shown for mean wave amplitude but is still quite broad because of the high occurrence rate found throughout the dayside. Time-averaged amplitudes at latitudes above 15° in the noon sector also appear much higher than those at dawn. Despite moderate characteristic amplitudes, the dusk sector distribution shows low time-averaged amplitudes because of the low observation rate, with time-averaged wave amplitudes of <3 pT throughout. Characterization of time-averaged wave regions culminates in a trend of increasing time-averaged amplitude, from midnight to dawn and then to

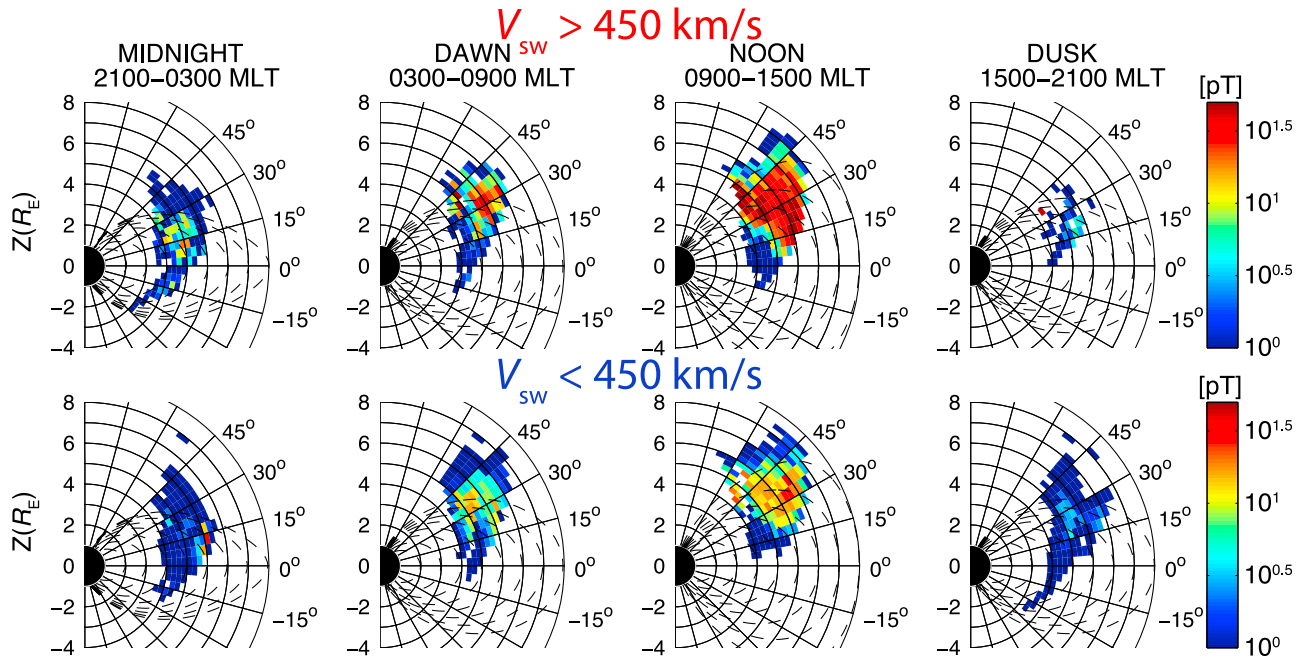

Figure 6. Solar wind speed dependence of time-averaged chorus wave amplitude.

noon, with the high-latitude boundary shifting from 15° to 45° and then to 50°.

[32] When the mean wave amplitude and occurrence rate distributions are effectively combined, or time intervals where no chorus was observed are included to produce time-averaged wave amplitude, a clear domination of the occurrence rate is imposed on the amplitude distribution. This can be seen by the confinement of intense waves at dawn and noon to well defined regions where probability of occurrence is high. This effect is most prominent at midnight and dusk, where, despite moderate mean amplitudes, time-averaged distributions appear confined to the equator at midnight and are severely suppressed at dusk.

3.5. Variation With Geomagnetic Activity

[33] Previously, *Bunch et al.* [2011] and *Sigsbee et al.* [2010] used Polar PWI data to explore the geomagnetic dependence of chorus spectral intensity and occurrence frequency, respectively. Here we examine the variation of time-averaged chorus amplitude with geomagnetic activity, as well as the relative influence of dynamic pressure, convection electric field, solar wind speed, substorm activity, and global disturbance level on chorus statistics. Figure 5 shows R–λ distributions of time-averaged wave amplitude for three levels of the auroral electrojet (AE) index. Intervals where $AE < 100$ nT, $100 < AE < 300$ nT, and $AE < 300$ nT comprise 51.2%, 32.1%, and 16.7% of the total study interval. Investigation of variation with AE*, the maximum AE value over the previous 3 h, results in the same trends. Figure 6 shows R–λ distributions of time-averaged wave amplitude for two levels of the solar wind speed (V_{SW}). Intervals where $V_{SW} < 450$ km/s and $V_{SW} > 450$, represent 63% and 37% of the total duration of this study. We find that for elevated levels of AE and V_{SW}, time-averaged wave amplitudes increase in the midnight, dawn and noon sectors. However, the relative change in time-averaged wave amplitude is higher at midnight, while significant amplitudes are observed at noon even under quiet conditions. At dusk, time-averaged wave amplitudes are significantly lower than other sectors but slightly increase with enhanced solar wind speed while decreasing for elevated AE.

Table 1. Mean Amplitude (MA) for High-Latitude (15°–45°, 4–8 R_E) Chorus Observations During Time Intervals Where a Given Activity Measure is Below (<) or Above (>) Its Median Value and the Change Δ of the Mean Amplitude From Below to Above the Median Activity Value

	Midnight			Dawn			Noon			Dusk		
	MA (pT)		Δ	MA (pT)		Δ	MA (pT)		Δ	MA (pT)		Δ
Median Value	<	>	(dB)	<	>	(dB)	<	>	(dB)	<	>	(dB)
Pressure = 2 nPa	12	13	+0.70	38	44	+1.3	58	53	−0.78	17	17	0.0
$V_{SW}B_s$* = 0.18 mV/m	11	13	+1.4	36	45	+1.9	63	51	−1.8	22	11	−6.0
V_{SW} = 380 km/s	6.4	15	+7.4	41	41	0.0	40	58	+3.2	18	16	−1.0
Kp = 1.7	6.7	15	+7.0	30	49	+4.3	48	61	+2.1	19	6.6	−9.2
AE = 100 nT	6.3	14	+6.9	31	48	+3.8	52	58	+0.95	19	8.3	−7.2

Table 2. Frequency of Occurrence (FO) of High-Latitude (15°–45°, 4–8 R_E) Chorus During Time Intervals Where a Given Activity Measure Is Above or Below Its Median Value and the Percent Change in Occurrence From Below to Above the Median Value

	Midnight			Dawn			Noon			Dusk		
	FO (%)		Δ	FO (%)		Δ	FO (%)		Δ	FO (%)		Δ
Median Value	<	>	(%)	<	>	(%)	<	>	(%)	<	>	(%)
Pressure = 2 nPa	5.3	6.1	+15	14	11	−27	23	24	+4.3	3.9	4.2	+8
$V_{SW}B_s$* = 0.18 mV/m	3.9	7.6	+95	16	13	−18	21	23	+9.5	4.2	2.7	−36
V_{SW} = 380 km/s	4.8	6.3	+31	9.7	16	+65	12	30	+150	4.8	3.1	−35
Kp = 1.7	2.8	8.1	+190	7.3	20	+170	15	30	+100	5.6	1.8	−68
AE = 100 nT	2.6	8.5	+230	9.2	17	+85	22	26	+92	6.1	1.8	−70

[34] Further quantification of the role of geomagnetic activity and solar wind parameters in controlling chorus mean amplitudes, occurrence rates, and time-averaged amplitudes is given in Tables 1, 2, and 3. We explore five different activity measures: solar wind dynamic pressure (P), "rectified" solar wind electric field averaged over the previous 30 min ($V_{SW}B_s$*, or solar wind speed times the absolute value of the southward component of the interplanetary magnetic field), solar wind speed (V_{SW}), geomagnetic activity (Kp), and substorm activity (AE) and present the change in chorus parameters above and below the median value of each activity measure.

[35] For example, each row of Table 1 shows the mean chorus amplitude for two levels of geomagnetic activity, above and below its median value, as well as the difference of the two amplitudes (in dB) for each MLT sector averaged across the region of maximal statistics (4 R_E < R < 8 R_E, 15° < λ < 45°). Focusing on the change in mean amplitude allows us to identify the relative importance of each parameter for each MLT sector. The most prominent trend appears to be the impact of V_{SW}, Kp, and AE at midnight where amplitudes increase by ~7 dB for chorus generated when V_{SW} > 380 km/s, Kp > 1.7, and AE > 100 nT. Dynamic pressure and $V_{SW}B_s$* have modest influences on mean amplitude (Δ < 6 dB for all MLT sectors). Solar wind speed, V_{SW} appears to impact amplitude at noon, but very little at dawn and dusk. Enhanced Kp and AE result in increased mean amplitude at dawn but decreased amplitude at dusk.

[36] Table 2 explores the impact of geomagnetic conditions on chorus occurrence statistics and is in the same format as Table 1. The influence of both P and $V_{SW}B_s$* on the occurrence rate of chorus appears modest (Δ < 100%), however the change in occurrence has opposite sign to that of mean amplitude for P and $V_{SW}B_s$* at dawn and noon. Increased V_{SW}, Kp, and AE correspond to significant increases in occurrence rate at midnight, dawn, and noon. In the dusk sector, an opposite trend to the rest of the magnetosphere is observed, where increased activity in V_{SW}, Kp, and AE correspond to sharp decreases in occurrence, but increased solar wind electric field and dynamic pressure have a positive effect.

[37] In the same format as Tables 1 and 2, Table 3 explores the impact of geomagnetic conditions on time-averaged chorus amplitude, determining the combined effect of changes in amplitude and occurrence. For instances of no change in mean amplitude or opposite sign to change in occurrence rate, the change in occurrence appears to dominate with the exception of one case. For this case, mean amplitude at noon decreases for increased dynamic pressure, and occurrence increases resulting in a slight decrease in time-averaged amplitude. Dramatic increases in mean amplitude and occurrence for increased V_{SW}, Kp, and AE result in increases in time-averaged amplitude at midnight, dawn, and noon of 4.2–16 dB, and decreases at dusk of 4.4–29 dB. This dominant influence of V_{SW}, Kp, and AE on chorus variation, and the similar pattern observed for each case, points to a potentially greater significance of general activity level rather than specific magnetospheric configurations due to parameters such as dynamic pressure.

4. Discussion

[38] As also suggested by previous work [*Tsurutani and Smith*, 1977; *Meredith et al.*, 2003c; *Li et al.*, 2009], in the off-equatorial (λ > 15°) magnetosphere at radial distances of 4–8 R_E, chorus waves have the highest occurrence rate, mean amplitude and time-averaged amplitude in the noon and dawn local time sectors. On the nightside in this region, chorus occurs infrequently and with lower amplitude. This is in contrast to the nightside equatorial region where the most intense magnetospheric chorus emissions can observed [*Li et al.*, 2011a]. These intense waves are confined to latitudes

Table 3. Time-Averaged Amplitude (TA) for High-Latitude (15°–45°, 4–8 R_E) Chorus During Time Intervals Where A Given Activity Measure Is Above or Below Its Median Value and the Variation in Amplitude From Below to Above the Median Value

	Midnight			Dawn			Noon			Dusk		
	TA (pT)		Δ	TA (pT)		Δ	TA (pT)		Δ	TA (pT)		Δ
Median Value	<	>	(dB)	<	>	(dB)	<	>	(dB)	<	>	(dB)
Pressure = 2 nPa	0.63	0.76	+1.6	5.4	4.9	−0.84	14	13	−0.64	0.65	0.73	+1.0
$V_{SW}B_s$* = 0.18 mV/m	0.44	0.97	+6.9	5.6	6.0	+0.60	13	11	−1.5	0.93	0.31	−9.5
V_{SW} = 380 km/s	0.31	0.93	+9.5	4.0	6.5	+4.2	4.3	17	+12	0.85	0.51	−4.4
Kp = 1.7	0.19	1.2	+16	2.2	9.5	+13	7.0	18	+8.2	1.1	0.12	−19
AE = 100 nT	0.15	1.0	+16	1.9	6.7	+11	9.2	18	+5.8	1.6	0.06	−29

of less than 15°–25° magnetic latitude [*Meredith et al.*, 2003c; *Bunch et al.*, 2011; *Li et al.*, 2011a].

[39] In the noon sector, observations by Polar show a relatively large spatial region with high wave occurrence, with rates of 15%–20% at latitudes extending above 45°. Waves on the dayside occur over a wider range of activity, and even during quiet conditions wave mean and time-averaged amplitudes at noon significantly exceed disturbance amplitudes at midnight (at least at latitudes of >15°). High occurrence in the noon sector is not fully understood [*Tsurutani et al.*, 2009; *Santolík et al.*, 2010; *Sigsbee et al.*, 2010; *Spasojevic and Inan*, 2010] but is likely a combination of several factors including higher magnetic field homogeneity and lower damping leading to superior generation or propagation conditions as well as additional contributions to chorus source energy aside from injected electrons. It has been suggested that this could be related to the local magnetospheric configuration because of solar wind speed or dynamic pressure [e.g., *Tsurutani and Smith*, 1977; *Koons and Roeder*, 1990; *Santolík et al.*, 2005b; *Li et al.*, 2009; *Spasojevic and Inan*, 2010]. Recent studies have shown that particles experiencing so-called Shabansky orbits, in which their drift motion shifts to high latitudes in the outer dayside [*Shabansky*, 1971], can lead to significant ion anisotropies and subsequently ion cyclotron wave growth in this region [*McCollough et al.*, 2010]. Whether Shabansky orbits can lead to electron anisotropies that contribute to chorus growth is currently under investigation. The low occurrence rate at dusk is expected and is likely due to the lifetimes and drift paths of the source electrons [*Lyons and Williams*, 1984] and may also be influenced by the extension of the plasmaspheric plume [*Spasojevic et al.*, 2003]. Despite the low occurrence rate, chorus was observed at some time during ~31% of half orbits traversing the dusk sector. In the dusk sector, observation of waves appears to be more limited to quiet conditions. However, when waves are present mean amplitudes at dusk exceed those at midnight and approach amplitudes observed in the dawn sector. Thus, how chorus is generated at dusk and the role that waves in this sector may play in radiation belt dynamics remains an open question. Study of MeV microbursts using SAMPEX has shown events to be more evenly distributed in MLT and extending toward dusk during quiet times [*O'Brien et al.*, 2003]. This is similar to the pattern we observe for off-equatorial chorus as it extends into the dusk sector primarily during quiet times.

[40] In our study of geomagnetic and solar wind, we find that simple measures of activity, such as the *Kp* index do remarkably well at predicting when wave occurrence, mean amplitude and time-averaged amplitude are expected to be high.

[41] It is also important to note that the problem of defining typical chorus characteristics, as they pertain to interaction with radiation belt particles, is only loosely resolved by the typical method of integrating wave power across the pertinent band and averaging over space and time. Chorus is a spontaneously generated emission, with RMS intensities that vary on the time scale of minutes to hours, and fine structures with variation at subsecond time scales. Moreover, for a given region in space, its importance to radiation belt modeling depends on several quantities: its frequency limits, characteristic RMS amplitude, power distribution across the band, and how often and under what conditions it is observed, as well as its characteristic fine structure and coherence. The impact of these parameters, with the exception of fine structure, can be modeled by QL diffusion calculations. Still, the impact of each of these characteristics must be modeled and interpreted carefully since both occurrence rate and typical observed amplitude both work to dictate the distribution of time-averaged wave power used by QL calculations. The importance of this point is illustrated by the distributions throughout Figure 4 as the distribution of intense waves shown in Figure 4c is reduced in space and amplitude for all time sectors after consideration of occurrence rate, as well as Tables 1–3 showing the relative importance of the dynamics of occurrence and amplitude for each region.

[42] Thus, the use of chorus amplitudes that are time-averaged over days, weeks, and months, as provided by time-averaged wave amplitude statistics by others and shown here in Figure 4d, provides a first-order picture for wave activity, whereas shorter time scale (e.g., hours to days) intervals of intense geomagnetic activity may be better modeled using wave distributions of mean amplitude, such as shown in Figure 4c. Moreover, a characteristic of chorus observed by Polar and illustrated in Figure 1a is that it is commonly observed for continuous intervals on ascending and descending traverses of the magnetosphere, and thus may often define a volume in space where chorus of significant amplitude is present throughout.

[43] The method of data analysis employed in this paper is different from those used in previous studies and carries with it a set of advantages and disadvantages that are important to note. The first advantage may be that visual inspection allows for the isolation of chorus for evaluation against other potential controllers of radiation belt electron flux (e.g., hiss, ULF, and EMIC waves), which does not depend on the accuracy of field line tracing to determine the correct chorus band. It allows for the rejection of electrostatic emissions by correlation filter, deletion of man made transmitters or interference, and avoidance of variable noise and other non-chorus emissions. The calculation of wave amplitude employed here introduces a systematic uncertainty, though this uncertainty is quantifiable, whereas error estimation using band integration may be less clear. Accuracy of manual selection, measurement precision/resolution, and method of extrapolation are further complications to consider.

[44] Measurement precision and frequency/time resolution are also inherent in any experiment. Compared to previous investigations of this type, the Polar SFR has similar frequency/time resolution to CRRES [*Meredith et al.*, 2001] and similar time but much higher frequency resolution than THEMIS wave instruments [*Li et al.*, 2009]. Observations used here from Polar use direct measurement of B above $\sim 10^{-13}$ nT^2/Hz and measured chorus at fractions of pT. This resulted in 23% of chorus events observed by Polar being below the detectability threshold of the CRRES and THEMIS studies (3 pT), though waves at these amplitudes may not significantly impact wave-particle models. CRRES studies used measurements of E and the cold plasma whistler dispersion relation to infer B [*Meredith et al.*, 2003b, 2003c], and THEMIS results by *Li et al.* [2009] used filter banks

with bandwidths comparable to that of the chorus being observed. These experiments resulted in the detectability of signals above $\sim 10^{-11}$ nT^2/Hz for THEMIS and $\sim 10^{-13}$ nT^2/Hz for CRRES [*Anderson et al.*, 1992; *Cully et al.*, 2008a].

[45] The above advantages in mind, we also point out the disadvantages of the methods used here. The first being the opposite argument to isolation of chorus emissions, in that the determination of electron diffusion rates in the radiation belts depends on wave amplitude and frequency alone. The nature of the emission and its characteristic band only identifies its relative contribution to acceleration and loss with respect to other drivers. Next, the systematic uncertainty introduced by the estimation of wave amplitude from spectral density may be as high as 40%, though this is smaller than the statistical uncertainty of observed amplitudes given by the standard deviation and interquartile range of the lognormal distributions, which are around 10^2 and $10^{0.5}$, respectively (e.g., Figure 3c of this paper and Figure 2 of *Horne et al.* [2005]). These data also primarily determine the RMS type intensities of chorus and do not resolve the variation in chorus coherence or short time scale structure [e.g., *Santolík et al.*, 2003; *Cully et al.*, 2008b; *Tsurutani et al.*, 2011].

[46] While the Polar SFR measurements used here, like those from CRRES and THEMIS, do not resolve the element and subelement structure of chorus, statistical determination of wave coherence properties will likely prove to be important for understanding the contributions of not just QL diffusive processes, but the impact of more discrete wave-particle interactions [*Tsurutani et al.*, 2009; *Lakhina et al.*, 2010; *Tsurutani et al.*, 2011] with coherent, semicoherent, and potentially very high amplitude waves [*Santolík et al.*, 2003; *Cully et al.*, 2008b]. In fact, *Tsurutani et al.* [2011] have recently shown using the Polar High Frequency Waveform Receiver (HFWR), which periodically collected short intervals of high-resolution data, that off-equatorial chorus can be less coherent than at the equator, but still more coherent than is assumed for application of QL theory, and that it may require yet a different approach from QL [*Schulz and Lanzerotti*, 1974] or transport [*Lakhina et al.*, 2010] theories to accurately model these wave-particle interactions.

[47] We finally point out that these statistics are also somewhat unique in that they are from a period of solar minimum. This has a significant impact on the occurrence of coronal mass ejection (CME) and high-speed stream driven storms, as well as the resulting magnetospheric configurations and substorm response. Thus, solar minimum may significantly bias occurrence rates and amplitudes shown here as lower than during other phases of the solar cycle, though more long-term statistical studies throughout the solar cycle will be needed to elicit such dependencies.

5. Conclusions

[48] The work presented here is the first statistical quantification of time-averaged chorus wave amplitude in the off-equatorial region. Because of the orbital constraints of the Polar spacecraft, our conclusions apply only to the region $15° < \lambda < 60°$, and $4\ R_E < R < 8\ R_E$.

[49] 1. Typical high-latitude chorus wave amplitudes derived in this study appear to occur most often in the tens of pT, and range into the hundreds of pT, consistent with previous observations made by CRRES and THEMIS at lower latitudes [*Meredith et al.*, 2001; *Li et al.*, 2007].

[50] 2. Both occurrence and mean amplitude statistics are highest in the dawn and noon time sectors, which results in the highest time-averaged amplitudes, and is also consistent with previous results for lower latitudes [*Tsurutani and Smith*, 1977; *Meredith et al.*, 2001, 2003c; *Li et al.*, 2009]. In the midnight sector, despite moderate mean amplitudes up to $\lambda \approx 30°$, time-averaged amplitudes are low because of the low occurrence rate, with the resulting distribution primarily confined to $\lambda < 15°$ also consistent with previous studies [*Tsurutani and Smith*, 1977; *Meredith et al.*, 2001, 2003c; *Li et al.*, 2009].

[51] 3. Despite the fact that occurrence rates and time-averaged amplitudes are low in the dusk sector, when the waves are present, amplitudes are fairly intense in the $15° < \lambda < 30°$ range. This has potential to be important for the scattering of >1 MeV electrons (see discussion by *Millan and Thorne* [2007]) and duskside microburst precipitation [*O'Brien et al.*, 2003], and further investigation of the conditions for wave growth in the dusk sector should be studied further.

[52] 4. Although waves are sometimes observed at $\lambda > 50°$ in the noon sector, time-averaged amplitude decreases rapidly above this latitude because of lower observation rates.

[53] 5. Time-averaged amplitudes at high latitudes in the noon sector (i.e., the dayside outer zone) appear to be significantly higher than those at dawn.

[54] 6. The noon sector shows both the greatest rate of observation maximizing near 50% for $\lambda < 45°$ and ranges to the outer radial edge of the orbit coverage.

[55] 7. The latitude to which significant time-averaged chorus amplitude appears to be confined shifts from 15° to 45° and to 50° from midnight to dawn to noon.

[56] In terms of chorus amplitude as a function of geomagnetic activity, the following conclusions were made.

[57] 1. For increasing *AE* and V_{SW} an increase in time-averaged amplitude is observed at midnight, dawn, and noon, while amplitude at dusk remains consistently low.

[58] 2. Occurrence rate distributions show similar trends to those of time-averaged wave amplitude and appear to have dominant control of the boundaries of time-averaged distributions.

[59] 3. Increased V_{SW} appears to correspond more strongly than *AE* with increased amplitude in the dayside outer zone.

[60] 4. Activity dependence is most dramatic at midnight, significant but less dramatic at dawn, and least dramatic at noon where amplitudes are high for all activity levels. This may be related to the relative influence of substorm injections at midnight and compression at noon.

[61] 5. Dusk sector chorus appears to have moderate amplitudes and occur most frequently during geomagnetically quiet times. This is similar to the occurrence pattern observed for duskside microburst precipitation [*O'Brien et al.*, 2003].

[62] 6. While magnetospheric configuration due to dynamic pressure appears to impact chorus characteristics, global geomagnetic activity indicated by *Kp*, V_{SW}, or *AE*

appear to more strongly correlate with high chorus amplitude and occurrence.

[63] **Acknowledgments.** The OMNI data were obtained from the GSFC/SPDF OMNIWeb. We thank D. Boscher, S. Bourdarie, P. O'Brien, and T. Guild for providing the ONERA-DESP library v4.2, Toulouse, France, 2004–2008, as well as Daniel Golden for helpful discussions. The *AE* and *Kp* indices were provided by the Kyoto World Data Center for Geomagnetism. This research was supported by the NASA Living With a Star Jack Eddy Postdoctoral Fellowship Program, administered by the UCAR Visiting Scientist Programs, as well as NASA grant NNX09AF51G.

[64] Robert Lysak thanks the reviewers for their assistance in evaluating this paper.

References

Albert, J. M. (1993), Cyclotron resonance in an inhomogeneous magnetic field, *Phys. Fluids B*, *5*(8), 2744–2750, doi:10.1063/1.860715.

Albert, J. M., and J. Bortnik (2009), Nonlinear interaction of radiation belt electrons with electromagnetic ion cyclotron waves, *Geophys. Res. Lett.*, *36*, L12110, doi:10.1029/2009GL038904.

Albert, J. M., N. P. Meredith, and R. B. Horne (2009), Three-dimensional diffusion simulation of outer radiation belt electrons during the 9 October 1990 magnetic storm, *J. Geophys. Res.*, *114*, A09214, doi:10.1029/2009JA014336.

Anderson, R. R., D. A. Gurnett, and D. L. Odem (1992), CRRES plasma wave experiment, *J. Spacecr. Rockets*, *29*(4), 570–573.

Bortnik, J., and R. M. Thorne (2007), The dual role of ELF/VLF chorus waves in the acceleration and precipitation of radiation belt electrons, *J. Atmos. Sol. Terr. Phys.*, *69*(3), 377–386, doi:10.1016/j.jastp.2006.05.030.

Bortnik, J., R. M. Thorne, and N. P. Meredith (2008), The unexpected origin of plasmaspheric hiss from discrete chorus emissions, *Nature*, *452*, 62–66, doi:10.1038/nature06741.

Bunch, N. L., M. Spasojevic, and Y. Y. Shprits (2011), On the latitudinal extent of chorus as observed by the Polar Plasma Wave Instrument, *J. Geophys. Res.*, *116*, A04204, doi:10.1029/2010JA016181.

Burtis, W. J., and R. A. Helliwell (1969), Banded chorus—A new type of VLF radiation observed in the magnetosphere by OGO 1 and OGO 3, *J. Geophys. Res.*, *74*(11), 3002–3010, doi:10.1029/JA074i011p03002.

Burtis, W. J., and R. A. Helliwell (1976), Magnetospheric chorus: Occurrence patterns and normalized frequency, *Planet. Space Sci.*, *24*(11), 1007–1010, doi:10.1016/0032-0633(76)90119-7.

Cattell, C., et al. (2008), Discovery of very large amplitude whistler mode waves in Earth's radiation belts, *Geophys. Res. Lett.*, *35*, L01105, doi:10.1029/2007GL032009.

Cully, C. M., R. E. Ergun, K. Stevens, A. Nammari, and J. Westfall (2008a), The THEMIS digital fields board, *Space Sci. Rev.*, *141*(1–4), 343–355, doi:10.1007/s11214-008-9417-1.

Cully, C. M., J. W. Bonnell, and R. E. Ergun (2008b), THEMIS observations of long lived regions of large amplitude whistler waves in the inner magnetosphere, *Geophys. Res. Lett.*, *35*, L17S16, doi:10.1029/2008GL033643.

Dunckel, N., and R. A. Helliwell (1969), Whistler mode emissions on the OGO 1 satellite, *J. Geophys. Res.*, *74*(26), 6371–6385, doi:10.1029/JA074i026p06371.

Friedel, R. H. W., G. D. Reeves, and T. Obara (2002), Relativistic electron dynamics in the inner magnetosphere—A review, *J. Atmos. Sol. Terr. Phys.*, *64*(2), 265–282, doi:10.1016/S1364-6826(01)00088-8.

Golden, D. I., M. Spasojevic, F. R. Foust, N. G. Lehtinen, N. P. Meredith, and U. S. Inan (2010), Role of the plasmapause in dictating the ground accessibility of ELF/VLF chorus, *J. Geophys. Res.*, *115*, A11211, doi:10.1029/2010JA015955.

Golden, D. I., M. Spasojevic, and U. S. Inan (2011), Determination of solar cycle variations of midlatitude ELF/VLF chorus and hiss via automated signal detection, *J. Geophys. Res.*, *116*, A03225, doi:10.1029/2010JA016193.

Golkowski, M., and U. S. Inan (2008), Multistation observations of ELF/VLF whistler mode chorus, *J. Geophys. Res.*, *113*, A08210, doi:10.1029/2007JA012977.

Gurnett, D. A., et al. (1995), The Polar Plasma Wave Instrument, *Space Sci. Rev.*, *71*(1–4), 597–622, doi:10.1007/BF00751343.

Haque, N., M. Spasojevic, O. Santolík, and U. S. Inan (2010), Wave normal angles of magnetospheric chorus emissions observed on the Polar spacecraft, *J. Geophys. Res.*, *115*, A00F07, doi:10.1029/2009JA014717.

Horne, R. B., and R. M. Thorne (2003), Relativistic electron acceleration and precipitation during resonant interactions with whistler-mode chorus, *Geophys. Res. Lett.*, *30*(10), 1527, doi:10.1029/2003GL016973.

Horne, R. B., S. A. Glauert, and R. M. Thorne (2003), Resonant diffusion of radiation belt electrons by whistler-mode chorus, *Geophys. Res. Lett.*, *30*(9), 1493, doi:10.1029/2003GL016963.

Horne, R. B., R. M. Thorne, S. A. Glauert, J. M. Albert, N. P. Meredith, and R. R. Anderson (2005), Timescale for radiation belt electron acceleration by whistler mode chorus waves, *J. Geophys. Res.*, *110*, A03225, doi:10.1029/2004JA010811.

Inan, U. S., T. F. Bell, and R. A. Helliwell (1978), Nonlinear pitch angle scattering of energetic electrons by coherent VLF waves in the magneto- sphere, *J. Geophys. Res.*, *83*(A7), 3235–3253, doi:10.1029/JA083iA07p03235.

Kennel, C., and H. Petschek (1966), Limit on stably trapped particle fluxes, *J. Geophys. Res.*, *71*(1), 1–28, doi:10.1029/JZ071i001p00001.

Koons, H. C., and J. L. Roeder (1990), A survey of equatorial magnetospheric wave activity between 5 and 8 R_E, *Planet. Space Sci.*, *38*(10), 1335–1341, doi:10.1016/0032-0633(90)90136-E.

Lakhina, G. S., B. T. Tsurutani, O. P. Verkhoglyadova, and J. S. Pickett (2010), Pitch angle transport of electrons due to cyclotron interactions with the coherent chorus subelements, *J. Geophys. Res.*, *115*, A00F15, doi:10.1029/2009JA014885.

Li, W., Y. Y. Shprits, and R. M. Thorne (2007), Dynamic evolution of energetic outer zone electrons due to wave-particle interactions during storms, *J. Geophys. Res.*, *112*, A10220, doi:10.1029/2007JA012368.

Li, W., R. M. Thorne, V. Angelopoulos, J. Bortnik, C. M. Cully, B. Ni, O. LeContel, A. Roux, U. Auster, and W. Magnes (2009), Global distribution of whistler-mode chorus waves observed on the THEMIS spacecraft, *Geophys. Res. Lett.*, *36*, L09104, doi:10.1029/2009GL037595.

Li, W., J. Bortnik, R. M. Thorne, and V. Angelopoulos (2011a), Global distribution of wave amplitudes and wave normal angles of chorus waves using THEMIS wave observations, *J. Geophys. Res.*, *116*, A12205, doi:10.1029/2011JA017035.

Li, W., R. M. Thorne, J. Bortnik, Y. Y. Shprits, Y. Nishimura, V. Angelopoulos, C. Chaston, O. Le Contel, and J. W. Bonnell (2011b), Typical properties of rising and falling tone chorus waves, *Geophys. Res. Lett.*, *38*, L14103, doi:10.1029/2011GL047925.

Li, X., D. N. Baker, M. Temerin, D. Larson, R. P. Lin, G. D. Reeves, M. Looper, S. G. Kanekal, and R. A. Mewaldt (1997), Are energetic electrons in the solar wind the source of the outer radiation belt?, *Geophys. Res. Lett.*, *24*(8), 923–926, doi:10.1029/97GL00543.

Li, X., D. N. Baker, S. G. Kanekal, M. Looper, and M. Temerin (2001), Long term measurements of radiation belts by SAMPEX and their variations, *Geophys. Res. Lett.*, *28*(20), 3827–3830, doi:10.1029/2001GL013586.

Lorentzen, K. R., J. B. Blake, U. S. Inan, and J. Bortnik (2001), Observations of relativistic electron microbursts in association with VLF chorus, *J. Geophys. Res.*, *106*(A4), 6017–6027, doi:10.1029/2000JA003018.

Lyons, L. R., and D. J. Williams (1984), *Quantitative Aspects of Magnetospheric Physics*, Kluwer Acad., Hingham, Mass.

McCollough, J. P., S. R. Elkington, M. E. Usanova, I. R. Mann, D. N. Baker, and Z. C. Kale (2010), Physical mechanisms of compressional EMIC wave growth, *J. Geophys. Res.*, *115*, A10214, doi:10.1029/2010JA015393.

McIlwain, C. E. (1966), Magnetic coordinates, *Space Sci. Rev.*, *5*(5), 585–598.

Menietti, J. D., O. Santolík, and P. C. Abaci (2009), Chorus observations by the Polar spacecraft near the mid-altitude cusp, *Planet. Space Sci.*, *57*, 1412–1418, doi:10.1016/j.pss.2009.07.003.

Mellott, M. M., R. L. Huff, and D. A. Gurnett (1986), DE 1 observations of harmonic auroral kilometric radiation, *J. Geophys. Res.*, *91*(A12), 13,732–13,738.

Meredith, N. P., R. B. Horne, and R. R. Anderson (2001), Substorm dependence of chorus amplitudes: Implications for the acceleration of electrons to relativistic energies, *J. Geophys. Res.*, *106*(A7), 13,165–13,178.

Meredith, N. P., R. B. Horne, D. Summers, R. M. Thorne, R. H. A. Iles, D. Heynderickx, and R. R. Anderson (2003a), Evidence for acceleration of outer zone electrons to relativistic energies by whistler mode chorus, *Ann. Geophys.*, *20*, 967–979.

Meredith, N. P., M. Cain, R. B. Horne, R. M. Thorne, D. Summers, and R. R. Anderson (2003b), Evidence for chorus-driven electron acceleration to relativistic energies from a survey of geomagnetically disturbed periods, *J. Geophys. Res.*, *108*(A6), 1248, doi:10.1029/2002JA009764.

Meredith, N. P., R. B. Horne, R. M. Thorne, and R. R. Anderson (2003c), Favored regions for chorus-driven electron acceleration to relativistic energies in the Earth's outer radiation belt, *Geophys. Res. Lett.*, *30*(16), 1871, doi:10.1029/2003GL017698.

Millan, R. M., and R. M. Thorne (2007), Review of radiation belt relativistic electron losses, *J. Atmos. Sol. Terr. Phys.*, *69*(3), 362–377, doi:10.1016/j.jastp.2006.06.019.

Mosier, S., M. Kaiser, and L. Brown (1973), Observations of noise bands associated with the upper hybrid resonance by the Imp 6 radio astronomy

experiment, *J. Geophys. Res.*, *78*(10), 1673–1679, doi:10.1029/JA078i010p01673.

Ni, B., R. M. Thorne, Y. Y. Shprits, and J. Bortnik (2008), Resonant scattering of plasma sheet electrons by whistler-mode chorus: Contribution to diffuse auroral precipitation, *Geophys. Res. Lett.*, *35*, L11106, doi:10.1029/2008GL034032.

O'Brien, T. P., K. R. Lorentzen, I. R. Mann, N. P. Meredith, J. B. Blake, J. F. Fennell, M. D. Looper, D. K. Milling, and R. R. Anderson (2003), Energization of relativistic electrons in the presence of ULF power and MeV microbursts: Evidence for dual ULF and VLF acceleration, *J. Geophys. Res.*, *108*(A8), 1329, doi:10.1029/2002JA009784.

O'Brien, T. P., M. D. Looper, and J. B. Blake (2004), Quantification of relativistic electron microburst losses during the GEM storms, *Geophys. Res. Lett.*, *31*, L04802, doi:10.1029/2003GL018621.

Orlova, K. G., and Y. Y. Shprits (2010), Dependence of pitch-angle scattering rates and loss timescales on the magnetic field model, *Geophys. Res. Lett.*, *37*, L05105, doi:10.1029/2009GL041639.

Qin, Z., R. E. Denton, N. A. Tsyganenko, and S. Wolf (2007), Solar wind parameters for magnetospheric magnetic field modeling, *Space Weather*, *5*, S11003, doi:10.1029/2006SW000296.

Reeves, G. D., K. L. McAdams, R. H. W. Friedel, and T. P. O'Brien (2003), Acceleration and loss of relativistic electrons during geomagnetic storms, *Geophys. Res. Lett.*, *30*(10), 1529, doi:10.1029/2002GL016513.

Roederer, J. G. (1970), *Dynamics of Geomagnetically Trapped Radiation*, *Phys. Chem. Space*, vol. 2, 166 pp., Springer, Berlin.

Russell, C. T., R. E. Holzer, and E. J. Smith (1969), OGO 3 observations of ELF noise in the magnetosphere: 1, Spatial extent and frequency of occurrence, *J. Geophys. Res.*, *74*(3), 755–777, doi:10.1029/JA074i003p00755.

Santolík, O., D. A. Gurnett, J. S. Pickett, M. Parrot, and N. Cornilleau-Wehrlin (2003), Spatio-temporal structure of storm-time chorus, *J. Geophys. Res.*, *108*(A7), 1278, doi:10.1029/2002JA009791.

Santolík, O., E. Macúšova, K. H. Yearby, N. Cornilleau-Wehrlin, and H. S. K. Alleyne (2005a), Radial variation of whistler-mode chorus: First results from the STAFF/DWP instrument on board the Double Star TC-1 spacecraft, *Ann. Geophys.*, *23*, 2937–2942, doi:10.5194/angeo-23-2937-2005.

Santolík, O., D. A. Gurnett, J. S. Pickett, M. Parrot, and N. Cornilleau-Wehrlin (2005b), Central position of the source region of storm-time chorus, *Planet. Space Sci.*, *53*, 299–305, doi:10.1016/j.pss.2004.09.056.

Santolík, O., E. Macúšova, E. E. Titova, B. V. Kozelov, D. A. Gurnett, J. S. Pickett, V. Y. Trakhtengerts, and A. G. Demekhov (2008), Frequencies of wave packets of whistler-mode chorus inside its source region: A case study, *Ann. Geophys.*, *26*, 1665–1670, doi:10.5194/angeo-26-1665-2008.

Santolík, O., J. S. Pickett, D. A. Gurnett, J. D. Menietti, B. T. Tsurutani, and O. Verkhoglyadova (2010), Survey of Poynting flux of whistler mode chorus in the outer zone, *J. Geophys. Res.*, *115*, A00F13, doi:10.1029/2009JA014925.

Sazhin, S. S., and M. Hayakawa (1992), Magnetospheric chorus emissions—A review, *Planet. Space Sci.*, *40*(5), 681–697, doi:10.1016/0032-0633(92)90009-D.

Schulz, M., and L. J. Lanzerotti (1974), *Particle Diffusion in the Radiation Belts*, *Phys. Chem. Space*, vol. 7, 215 pp., Springer, Berlin.

Shabansky, V. P. (1971), Some processes in the magnetosphere, *Space Sci. Rev.*, *12*(3), 299–418, doi:10.1007/BF00165511.

Shprits, Y. Y., R. M. Thorne, R. B. Horne, and D. Summers (2006), Bounce-averaged diffusion coefficients for field-aligned chorus waves, *J. Geophys. Res.*, *111*, A10225, doi:10.1029/2006JA011725.

Shprits, Y. Y., N. P. Meredith, and R. M. Thorne (2007), Parameterization of radiation belt electron loss timescales due to interactions with chorus waves, *Geophys. Res. Lett.*, *34*, L11110, doi:10.1029/2006GL029050.

Shprits, Y. Y., S. R. Elkington, N. P. Meredith, and D. A. Subbotin (2008a), Review of modeling of losses and sources of relativistic electrons in the outer radiation belt: I. Radial transport, *J. Atmos. Sol. Terr. Phys.*, *70*(14), 1679–1693, doi:10.1016/j.jastp.2008.06.008.

Shprits, Y. Y., D. A. Subbotin, N. P. Meredith, and S. R. Elkington (2008b), Review of modeling of losses and sources of relativistic electrons in the outer radiation belt: II. Local acceleration and loss, *J. Atmos. Sol. Terr. Phys.*, *70*(14), 1694–1713, doi:10.1016/j.jastp.2008.06.014.

Sigsbee, K., J. D. Menietti, O. Santolík, and J. B. Blake (2008), Polar PWI and CEPPAD observations of chorus emissions and radiation belt electron acceleration: Four case studies, *J. Atmos. Sol. Terr. Phys.*, *70*(14), 1774–1788, doi:10.1016/j.jastp.2008.02.005.

Sigsbee, K., J. D. Menietti, O. Santolík, and J. S. Pickett (2010), Locations of chorus emissions observed by the Polar Plasma Wave Instrument, *J. Geophys. Res.*, *115*, A00F12, doi:10.1029/2009JA014579.

Spasojevic, M., and U. S. Inan (2010), Drivers of chorus in the outer dayside magnetosphere, *J. Geophys. Res.*, *115*, A00F09, doi:10.1029/2009JA014452.

Spasojevic, M., J. Goldstein, D. L. Carpenter, U. S. Inan, B. R. Sandel, M. B. Moldwin, and B. W. Reinisch (2003), Global response of the plasmasphere to a geomagnetic disturbance, *J. Geophys. Res.*, *108*(A9), 1340, doi:10.1029/2003JA009987.

Subbotin, D., Y. Shprits, and B. Ni (2010), Three-dimensional VERB radiation belt simulations including mixed diffusion, *J. Geophys. Res.*, *115*, A03205, doi:10.1029/2009JA015070.

Summers, D. (2005), Quasi-linear diffusion coefficients for field-aligned electromagnetic waves with applications to the magnetosphere, *J. Geophys. Res.*, *110*, A08213, doi:10.1029/2005JA011159.

Summers, D., B. Ni, and N. P. Meredith (2007), Timescales for radiation belt electron acceleration and loss due to resonant wave-particle interactions: 2. Evaluation for VLF chorus, ELF hiss, and electromagnetic ion cyclotron waves, *J. Geophys. Res.*, *112*, A04207, doi:10.1029/2006JA011993.

Thorne, R. M. (2010), Radiation belt dynamics: The importance of wave-particle interactions, *Geophys. Res. Lett.*, *37*, L22107, doi:10.1029/2010GL044990.

Thorne, R. M., E. J. Smith, R. K. Burton, and R. E. Holzer (1973), Plasmaspheric hiss, *J. Geophys. Res.*, *78*(10), 1581–1596, doi:10.1029/JA078i010p01581.

Thorne, R. M., T. P. O'Brien, Y. Y. Shprits, D. Summers, and R. B. Horne (2005), Timescale for MeV electron microburst loss during geomagnetic storms, *J. Geophys. Res.*, *110*, A09202, doi:10.1029/2004JA010882.

Trakhtengerts, V. Y., A. G. Demekhov, E. E. Titova, B. V. Kozelov, O. Santolík, E. Macúšova, D. Gurnett, J. S. Pickett, M. J. Rycroft, and D. Nunn (2007), Formation of VLF chorus frequency spectrum: Cluster data and comparison with the backward wave oscillator model, *Geophys. Res. Lett.*, *34*, L02104, doi:10.1029/2006GL027953.

Tsurutani, B., and E. Smith (1974), Postmidnight chorus: A substorm phenomenon, *J. Geophys. Res.*, *79*(1), 118–127, doi:10.1029/JA079i001p00118.

Tsurutani, B., and E. Smith (1977), Two types of magnetospheric ELF chorus and their substorm dependences, *J. Geophys. Res.*, *82*(32), 5112–5128, doi:10.1029/JA082i032p05112.

Tsurutani, B. T., O. P. Verkhoglyadova, G. S. Lakhina, and S. Yagitani (2009), Properties of dayside outer zone chorus during HILDCAA events: Loss of energetic electrons, *J. Geophys. Res.*, *114*, A03207, doi:10.1029/2008JA013353.

Tsurutani, B. T., B. J. Falkowski, O. P. Verkhoglyadova, J. S. Pickett, O. Santolík, and G. S. Lakhina (2011), Quasi-coherent chorus properties: 1. Implications for wave-particle interactions, *J. Geophys. Res.*, *116*, A09210, doi:10.1029/2010JA016237.

Tsyganenko, N. A., and M. I. Sitnov (2005), Modeling the dynamics of the inner magnetosphere during strong geomagnetic storms, *J. Geophys. Res.*, *110*, A03208, doi:10.1029/2004JA010798.

Vaivads, A., O. Santolík, G. Stenberg, M. Andre, C. J. Owen, P. Canu, and M. Dunlop (2007), Source of whistler emissions at the dayside magnetopause, *Geophys. Res. Lett.*, *34*, L09106, doi:10.1029/2006GL029195.

N. L. Bunch and M. Spasojevic, Space, Telecommunications, and Radioscience Laboratory, Department of Electrical Engineering, Stanford University, 350 Serra Mall, Stanford, CA 94305, USA. (nbunch@stanford.edu)

Y. Y. Shprits, Institute of Geophysics and Planetary Physics, University of California, Los Angeles, CA 90095, USA.